MDPI

Article

Impacts of Wildlife Artificial Water Provisioning in an African Savannah Ecosystem: A Spatiotemporal Analysis

Morati Mpalo *[ID], **Lenyeletse Vincent Basupi** [ID] **and Gizaw Mengistu Tsidu** [ID]

Department of Earth and Environmental Science, Botswana International University of Science and Technology, Private Bag 16, Palapye, Botswana; basupiv@biust.ac.bw (L.V.B.); mengistug@biust.ac.bw (G.M.T.)
* Correspondence: mm21100016@studentmail.biust.ac.bw

Abstract: The use of artificial water points for wildlife in African savannah ecosystems has been widely criticised for affecting the distribution of wildlife and initiating changes in the heterogeneity of natural landscapes. We examined the spatiotemporal variations in the landscape before and after the installation of an artificial water point by integrating the analysis of vegetation and soil spectral response patterns with a supervised learning random forest model between 2002 and 2022 in Chobe Enclave, Northern Botswana. Our results revealed that the study area is characterised by animal species such as *Equus quagga*, *Aepyceros melampus*, and *Loxodonta africana*. The findings also showed that the main vegetation species in the study area landscape include *Combretum elaeagnoides*, *Vachellia luederitzii*, and *Combretum hereroense*. The artificial water point induced disturbances on a drought-vulnerable landscape which affected vegetation heterogeneity by degrading the historically dominant vegetation cover types such as *Colophospermum mopane*, *Dichrostachys cinerea*, and *Cynodon dactylon*. The immediate years following the artificial water point installation demonstrated the highest spectral response patterns by vegetation and soil features attributed to intense landscape disturbances due to abrupt high-density aggregation of wildlife around the water point. Landscapes were strongly homogenised in later years (2022), as shown by overly overlapping spectral patterns owing to an increase in dead plant-based material and senescent foliage due to vegetation toppling and trampling. The landscape disturbances disproportionately affected mopane-dominated woodlands compared to other vegetation species as indicated by statistically significant land cover change obtained from a random forest classification. The woodlands declined significantly ($p < 0.05$) within 0–0.5 km, 0.5–1 km, 1–5 km, and 5–10 km distances after the installation of the water point. The results of this study indicate that continuous nonstrategic and uninformed use of artificial water points for wildlife will trigger ecological alterations in savannah ecosystems.

Keywords: artificial water point; botswana; landsat; random forest; spectral response pattern; vegetation heterogeneity

1. Introduction

Artificially altering water availability in sub-tropical savannah ecosystems can affect herbivore distribution [1] and intensify their impacts on natural landscapes, particularly vegetation [2]. In this study, we aim to contribute to the understanding of the impacts of artificial water points (AWPs) on woody vegetation and soil conditions using one available AWP in the Chobe Enclave (CE) as a reference point for multitemporal analysis of landscape changes in the enclave. The adoption and implementation of artificial water sources worldwide have primarily focused on supplementing shortages of natural surface water [3]. In Botswana, the AWPs were initially intended to mitigate surface water scarcity in rangelands and facilitate livestock production through borehole schemes [3–5]. Their use was expanded in the 1980s to provide water to wildlife due to highly limited perennial surface water sources [6]. The interventions were also seen as important wildlife management strategies to minimise die-offs and optimise their utilisation of available forage [7].

This saw the government of Botswana installing AWPs mainly in protected areas such as the Central Kalahari Game Reserve (CKGR) [6]. In contrast, tourist enterprises have since adopted water supplementation methods to boost wildlife numbers around their premises and increase tourist visitation and satisfaction through enhanced wildlife viewing [8–10]. This has been noted to cause high-density aggregation of wildlife species around AWPs [8].

The concentration of some wildlife species, such as *Loxodonta africana*, can alter natural landscapes by causing homogenisation of foraging habitats, especially woody vegetation, thereby threatening biodiversity and ecosystem resilience [8,11,12]. However, little is known about the effects of wildlife densities on landscape changes through the utilisation of geospatial tools [12]. Previous studies have investigated AWPs in the tropical ecosystems of Botswana [7,9,13]; however, no similar studies have been conducted using geospatial tools to estimate the effects of increased wildlife concentrations on woody vegetation and soil. This is despite the advantage of the geospatial technologies to provide fine spatial resolution and high temporal resolution data that can simplify the quantification of landscape changes under AWPs [12]. Additionally, all previous studies have not been able to directly compare the landscape before and after the impact rather than inferring AWP-induced disturbances from the present spatial patterns alone.

In this study, we addressed the research gaps and limited scope of the previous studies since the multitemporal nature of satellite imageries allows for a more robust investigation of spatiotemporal disturbances induced by AWP. Our study area, in Northern Botswana, has the highest concentration of herbivore wildlife species including *Loxodonta africana*, *Syncerus caffer*, *Aepyceros melampus*, *Connochaetes taurinus*, *Kobus leche*, and *Equus quagga* [14]. The population of some of the species, for example, buffalos, zebras, impalas, wildebeests, and lechwe has been increasing over the years [14]. Some of these, for example, wildebeests, have residential inclinations around water sources and the creation of artificial water points affects the dynamics of their space use while also increasing their negative impacts on the surrounding vegetation [10]. The artificial points also tend to be dominated by water-dependent species such as impalas, zebras, and elephants to the detriment of some drought-tolerant species as they suffer from competition for forage [15]. They further influence localised changes in vegetation structure due to the increase in wildlife browsing and occupancy closer to the water points [16].

We, therefore, coupled the analysis of spectral response patterns of vegetation and soil features over time and supervised learning based on the random forest (RF) model in a Google Earth Engine to assess the temporal and spatial variations in landscapes around an AWP in CE. Our study achieved this aim through the following objectives:

1. Assessing wildlife and vegetation diversity in the study area.
2. Analysing the temporal conditions of vegetation and soil features before and after the installation of the AWP.

2. Materials and Methods

2.1. Study Area

The study area is the Chobe enclave, in the Chobe district of Botswana (Figure 1). It is a communally administered wildlife management area with a mixture of land uses comprising arable land and cattle posts. The area is semiarid to sub-humid [17] and characterised by intensive tourism activities [18,19]. It experiences an annual average rainfall of 600 mm with daily minimum and maximum temperatures of 6 °C and 22 °C, respectively [19]. Spatiotemporal variations in vegetation and soil conditions were assessed around an AWP located at 24.390855° E and −18.202900° S in CE (Figure 1). The AWP was introduced by a private safari operator in 2016 and has influenced wildlife visits and movements to the outskirts of a bush lodge in search of water. The AWP is near the Chobe Forest Reserve, and it is the only one available in the CE. It is in a transit zone between the forest reserve (which serves as a wildlife habitat) and the perennial Chobe River (Figure 1), thereby altering wildlife movements between the habitat and the river.
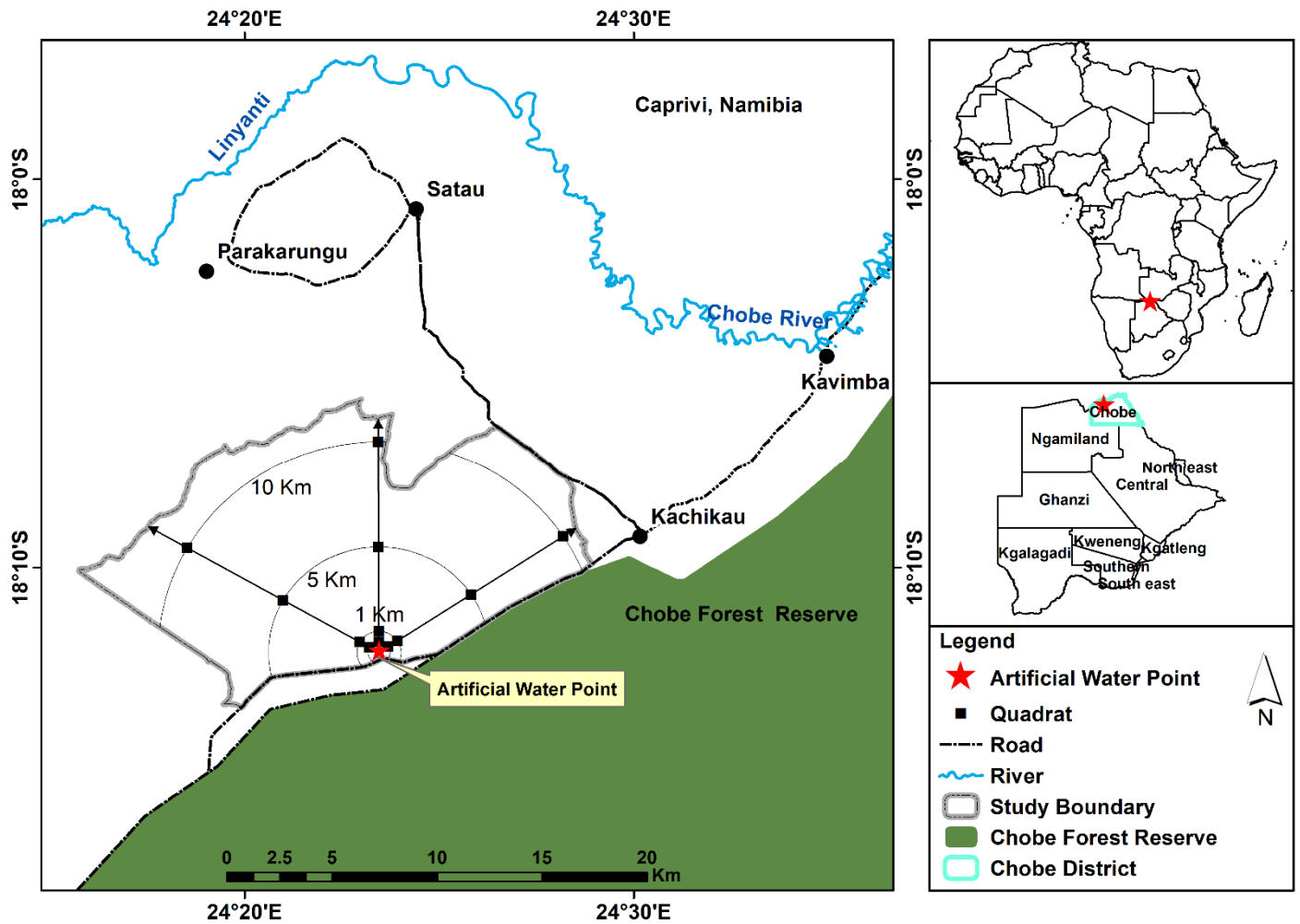
Figure 1. Map of the study area.

The location of CE settlements, namely Kavimba, Kachikau, Satau, and Parakarungu (Figure 1) also separates the wildlife habitat from the Chobe River, thereby limiting their access to the river and reducing their impacts around the natural water source.

Soils in the CE area are characterised by arenosols and gleysols, with a calcic horizon in the subsoil [19,20]. The soil supports vegetation communities that include diverse species, such as perennial swamp vegetation, annually flooded grasslands, broad and fine-leaved savannas, woodlands, and forests [19]. At the same time, a rich diversity of mega-herbivores characterises the enclave [21,22]. Wildlife displays free-range movements [23] characterised by seasonal shifts based on water availability, with dry season movements concentrating near perennial rivers and water sources [19].

2.2. Field Data and Sampling

Two field visits were used to collect ground data on land cover in the CE in April 2021 and April 2022. GPS (global position system)-guided transect walks radiating from the water source were used to study vegetation species and animal traces around the AWP. The transects were used to study vegetation species and animal traces in an area covering 187.2 km^2. Only three transects, radiating north-westerly, northerly, and north-easterly, were used (Figure 1). The southern directions of AWP were not sampled as the areas are occupied by the Chobe Forest Reserve and the Chobe National Park which already serve as wildlife conservation areas and habitats. As such, the transects were used to assess spatiotemporal variations in landscapes due to the encroachment of wildlife species influenced by the manipulation of surface water availability in a non-wildlife conservation

area. The transect method is frequently used in flora and fauna studies as it ensures spatial representativeness of sampled data by enabling more ground coverage in a given time [24,25]. Plots measuring 50 m × 50 m were systematically placed along the transects at 0.5 km, 1 km, 5 km, and 10 km from the AWP to study woody trees (i.e., plants ≥ 3 m in height, Figure 1). Within the 50 m × 50 m plots, 5 m × 5 m subplots were set up to study shrub and herbaceous cover species. Each 50 m × 50 m plot contained five (5) subplots 5 m × 5 m in size. A total of 12 plots were used to study woody tree species, and 60 subplots were used to study shrubs and herbs. According to Barnett and Stohlgren [26], large plots such as 50 m × 50 m are effective in providing a good picture of local vegetation conditions as well as enabling representative registering of species present in the area studied [27]. On the other hand, subplots of 5 m × 5 m were chosen as they facilitate the understanding of broad-scale landscape patterns [26]. Species names, counts, landscape disturbances, and land uses were observed in all plots. The Shannon–Wiener diversity index was used to estimate species diversity in the study area.

Animal species sighted at the different radii (i.e., 0.5 km, 1 km, 5 km, and 10 km) along the study transects were recorded based on the common species in Table 1 below to characterise common species within the periphery of the AWP. Other animal species that visited the AWP were identified from their spoors, droppings, and carcass remains within the 50 m × 50 m plots.

Table 1. Common animal and plant species in the study area and their categories of protection in the Red books.

Animal	Order	Family	English Name	Categories of Protection		
				International	Regional	National
Equus quagga Boddaert, 1785	Perissodactyla	Equidae	Plains zebra	Near threatened	Least concern	Not evaluated
Struthio camelus Linnaeus, 1758	Struthioniformes	Struthionidae	Ostrich	Least concern	Least concern	Not evaluated
Giraffa camelopardalis Linnaeus, 1758	Artiodactyla	Giraffidae	Giraffe	Vulnerable	Least concern	Not evaluated
Tragelaphus oryx Pallas, 1766	Artiodactyla	Bovidae	Common eland	Least concern	Least concern	Not evaluated
Helogale parvula Sundevall, 1847	Carnivora	Herpestidae	Common dwarf mongoose	Least concern	Least concern	Not evaluated
Mungos mungo Gmelin, 1788	Carnivora	Herpestidae	Banded mongoose	Least concern	Least concern	Not evaluated
Cynictis penicillata Cuvier, 1829	Carnivora	Herpestidae	Yellow mongoose	Least concern	Least concern	Not evaluated
Aepyceros melampus Lichtenstein, 1812	Artiodactyla	Bovidae	Impala	Least concern	Least concern	Not evaluated
Syncerus caffer Sparrman, 1779	Artiodactyla	Bovidae	African buffalo	Near threatened	Least concern	Not evaluated
Connochaetes taurinus Lichtenstein, 1812	Artiodactyla	Bovidae	Common wildebeest	Least concern	Least concern	Not evaluated
Loxodonta africana Blumenbach, 1797	Proboscidea	Elephantidae	African savanna elephant	Endangered	Least concern	Vulnerable
Phacochoerus africanus Gmelin, 1788	Artiodactyla	Suidae	African warthog	Least concern	Least concern	Not evaluated
Hippotragus equinus Desmarest, 1804	Artiodactyla	Bovidae	Roan antelope	Least concern	Endangered	Not evaluated
Tragelaphus strepsiceros Pallas, 1766	Artiodactyla	Bovidae	Greater kudu	Least concern	Least concern	Not evaluated
Canis mesomelas Schreber, 1775	Carnivora	Canidae	Black-backed jackal	Least concern	Least concern	Not evaluated
Crocuta crocuta Erxleben, 1777	Carnivora	Hyaenidae	Spotted hyena	Least concern	Least concern	Not evaluated
Panthera leo Linnaeus, 1758	Carnivora	Felidae	Lion	Vulnerable	Least concern	Vulnerable
Plants						
Eragrostis rigidior Pilg, 1912	Poales	Poaceae	Broad curly leaf	Not evaluated	Least concern	Not evaluated
Aristida junciformis Trin & Rupr, 1842	Poales	Poaceae	Wiregrass	Not evaluated	Least concern	Not evaluated
Heteropogon contortus (L) P.Beauv. ex Roem. & Schult 1817	Poales	Poaceae	Black spear grass	Not evaluated	Least concern	Not evaluated
Eragrostis pallens Hack, 1895	Poales	Poaceae	Broom love grass	Not evaluated	Least concern	Not evaluated
Cynodon dactylon Pers, 1805	Poales	Poaceae	Couch grass	Not evaluated	Least concern	Not evaluated
Megathyrsus maximus (Jacq.) B.K.Simon & S.W.L.Jacobs, 2003	Poales	Poaceae	Guinea grass	Not evaluated	Not evaluated	Not evaluated
Digitaria eriantha Steud, 1829	Poales	Poaceae	Common finger grass	Not evaluated	Least concern	Not evaluated
Ocimum americanum L, 1755	Lamiales	Lamiaceae	American basil	Not evaluated	Least concern	Not evaluated
Brachiaria dura Stapf, 1919	Poales	Poaceae	Signal grass	Not evaluated	Data-deficient	Not evaluated
Urochloa trichopus (Hochst.) Stapf, 1920	Poales	Poaceae	Bushveld signal grass	Not evaluated	Least concern	Not evaluated
Chloris virgata Sw, 1797	Poales	Poaceae	Feather finger grass	Not evaluated	Least concern	Not evaluated
Euclea divinorum Hiern, 1873	Ericales	Ebenaceae	Diamond-leaved Euclea	Not evaluated	Least concern	Not evaluated
Cyanthillium cinereum (L.) H.Rob, 1990	Asterales	Asteraceae	Little ironweed	Not evaluated	Not evaluated	Not evaluated
Geigeria alata (Hochst. & Steud. ex DC.) Benth. & Hook.fil. ex Oliv. & Hiern, 1877	Asterales	Asteraceae	Wing vomit daisy	Not evaluated	Not evaluated	Not evaluated
Dicoma tomentosa Cass, 1818	Asterales	Asteraceae	Woolly dicoma	Not evaluated	Least concern	Not evaluated
Cymbopogon caesius (Hook. & Arn.) Stapf, 1906	Poales	Poaceae	Kachi grass	Not evaluated	Least concern	Not evaluated
Rhus tenuinervis Engl, nd	Sapindales	Anacardiaceae	Commiphora rhus	Not evaluated	Not evaluated	Not evaluated
Croton gratissimus Burch, 1824	Malpighiales	Euphorbiaceae	Lavender croton	Least concern	Least concern	Not evaluated
Aristida adscensionis L, 1753	Poales	Poaceae	Six weeks threeawn	Not evaluated	Least concern	Not evaluated
Leonotis nepetifolia (L.) R.Br, 1811	Lamiales	Lamiaceae	Christmas candlestick	Not evaluated	Least concern	Not evaluated

Table 1. *Cont.*

Plants	Order	Family	English Name	Categories of Protection		
				International	Regional	National
Sesamum triphyllum Welw. ex Asch, 1889	Lamiales	Pedaliaceae	Wild sesame	Not evaluated	Least concern	Not evaluated
Schmidtia pappophoroides Steud. ex J.A.Schmidt, 1852	Poales	Poaceae	Kalahari sand quick	Not evaluated	Least concern	Not evaluated
Vachellia tortilis (Forssk.) Galasso & Banfi, 2008	Fabales	Fabaceae	Umbrella thorn	Least concern	Least concern	Not evaluated
Colophospermum mopane (J.Kirk ex Benth.) J.Léonard, 1949	Fabales	Fabaceae	Mopane	Least concern	Least concern	Not evaluated
Combretum elaeagnoides Klotzsch, 1861	Myrtales	Combretaceae	Large-fruited jesse-bush combretum	Least concern	Not evaluated	Not evaluated
Boscia albitrunca (Burch.) Gilg & Gilg-Ben, 1915	Brassicales	Capparaceae	Shepherd's tree	Least concern	Least concern	Not evaluated
Dichrostachys cinerea (L.) Wight & Arn 1834	Fabales	Fabaceae	Sickle bush	Least concern	Least concern	Not evaluated
Ziziphus mucronata Willd, 1809	Rosales	Rhamnaceae	Buffalo thorn	Least concern	Least concern	Not evaluated
Vachellia erioloba (E.Mey.) P.J.H.Hurter, 2008	Fabales	Fabaceae	Camel thorn	Least concern	Least concern	Not evaluated
Combretum hereroense Schinz, 1888	Myrtales	Combretaceae	Russet bushwillow	Least concern	Not evaluated	Not evaluated
Senegalia mellifera (Vahl) Seigler & Ebinger, 2010	Fabales	Fabaceae	Blackthorn	Least concern	Least concern	Not evaluated
Combretum imberbe Wawra, 1860	Myrtales	Combretaceae	Leadwood	Least concern	Least concern	Not evaluated
Vachellia hebeclada (DC.) Kyal. & Boatwr, 2013	Fabales	Fabaceae	Candle thorn	Least concern	Least concern	Data-deficient
Vachellia luederitzii (Engl.) Kyal & Boatwr, 2013	Fabales	Fabaceae	False umbrella thorn	Least concern	Least concern	Not evaluated
Senegalia galpinii (Burtt Davy) Seigler & Ebinger, 2010	Fabales	Fabaceae	Monkey-thorn	Least concern	Least concern	Not evaluated
Philenoptera violacea (Klotzsch) Schrire, 2000	Fabales	Fabaceae	Apple-leaf/ rain-tree	Least concern	Least concern	Not evaluated
Senegalia nigrescens (Oliv.) P.J.H.Hurter, 2008	Fabales	Fabaceae	Knob thorn	Not evaluated	Least concern	Not evaluated

Source: IUCN Red List of Threatened Species, Red List of South African Plants, Red List of South African Species, Botswana Plant Red Data List.

2.3. Satellite Imagery

Landsat imagery of sensors corresponding to the years 2002, 2012, 2018, 2020, and 2022 was obtained from the United States Geological Survey (USGS) portal as described in Table 2. Landsat collection 2, tier 1 images containing surface reflectance of land features, were obtained. Wet season satellite images were obtained to necessitate the detection of vegetation in its optimal growth. As such, Landsat images acquired in April were obtained across the study dates, as the month marks the end of the wet season in CE; hence, the optimal biomass was expected. Earlier dates images, i.e., 2002 and 2012, were used to assess spatiotemporal variations in vegetation and soil conditions 10 years before the construction of the AWP, while recent dates images, i.e., 2018, 2020, and 2022, were used to assess the conditions 6 years after the AWP on a 2-year interval. In this case, the satellite image for 2022 in the study area served as a reference image based upon which the RF model is trained using collected ground samples. The near-infrared band of the PlanetScope Super Dove (PSB. SD) instrument at 3 metres spatial resolution was obtained for the same scene in 2022 from the Planet labs portal https://www.planet.com/ (accessed on the 18 October 2022) for purposes of enhancing the reference Landsat images before using them to train the RF model.

2.4. Image Pre-Processing and Enhancement

Image co-registration was used to co-register image scenes from earlier dates (2002, 2012, 2018, and 2020) to the 2022 reference image. Co-registration of images was performed in ERDAS Imagine version 16.7.0. Image scenes obtained through the OLI/TIRS instrument were then rescaled to 8-bit unsigned to align their pixel depth with ETM+ for standardised analysis of spectral response patterns of features. All images were also reprojected to UTM Zone 35S using ERDAS imaging software. Scan line errors in the ETM+ acquired image for 2012 were corrected using the fill no-data function in open-source QGIS version 3.22.12. The near-infrared band of the PlanetScope Super Dove (PSB. SD) instrument was used to perform a multisensor Ehlers fusion across all image scenes. This type of image

merging technique keeps the spectral properties of the image of interest while sharpening their spatial resolution using a higher resolution image [28,29]. As such, through this fusion technique, all Landsat images were resampled from their original 30 m spatial resolution to the Super Dove (PSB. SD) NIR band's 3 m resolution. This improved image feature identification by emphasising high-intensity changes and grey-level discontinuities between pixels in all images [29]. The fusion technique was also based on multiple intensity–hue–saturation (IHS) transforms and fast Fourier transforms (FFTs). The former enhanced features, colour, and spatial resolution [30], while the latter applied an adaptive filter to the images.

Table 2. Image specifications for Landsat 7 ETM+ and Landsat 8 OLI/TIRS sensors used in 2002, 2012, 2018, 2020, and 2022.

Image Date	Sensor	Spectral Bands	Wavelengths (μm)	Spatial Resolution (m)
2002 and 2012	Landsat 7 Enhanced Thematic Mapper Plus (ETM+)	Band 1—Blue	0.45–0.52	30
		Band 2—Green	0.53–0.61	30
		Band 3—Red	0.63–0.69	30
		Band 4—Near-Infrared (NIR)	0.78–0.90	30
		Band 5—Shortwave Infrared (SWIR) 1	1.55–1.75	30
		Band 6—Thermal	10.40–12.50	60 * (30)
		Band 7—Shortwave Infrared (SWIR) 2	2.08–2.35	30
		Band 8—Panchromatic	0.52–0.90	30
2018, 2020, and 2022	Landsat 8 Operational Land Imager (OLI) and Thermal Infrared Sensor (TIRS)	Band 2—Blue	0.45–0.51	30
		Band 3—Green	0.53–0.59	30
		Band 4—Red	0.64–0.67	30
		Band 5—Near-Infrared (NIR)	0.85–0.88	30
		Band 6—Shortwave Infrared (SWIR) 1	1.57–1.65	30
		Band 7—Shortwave Infrared (SWIR) 2	2.11–2.29	30
		Band 8—Panchromatic	0.50–0.68	15

2.5. Analysis of Vegetation and Soil Spectral Response Patterns around the AWP over Time

Spectral response patterns of vegetation and soil features over time were used as proxies for temporal variations in woody vegetation and soil conditions in the CE. The spectral response patterns of features in all images (i.e., 2002, 2012, 2018, 2020, and 2022) were assessed at the exact location of the main sampling plots (50 m × 50 m) used for ground sampling in 2022. As such, pseudocolour band combinations, single band displays, and model spectral curves for earth features as described by Lillesand et al. [31] were used to identify both vegetation and soil features in the enhanced satellite images of the study area. A minimum of 6 pixels representing vegetation and soil were sampled using ERDAS per land cover to extract reflectance values of the features in the visible and reflected infrared wavelengths in all images. The reflectance values of pixels representative of vegetation and soil were averaged and used to plot spectral response patterns of the features across visible and infrared wavelengths. Specifically, blue, green, red, NIR, SWIR$_1$, and SWIR$_2$ wavebands were used to plot the spectral response patterns. The blue band is useful for soil/vegetation discrimination and forest mapping [31]. The waveband measures reflected energy in part of the wavelengths (0.45 to 0.67 μm) where chlorophyll in plants strongly absorbs the energy for photosynthesis [31]. The green band measures the green reflectance peak of vegetation essential for monitoring plant health and differentiating plant types [32]. The red band detects the strongest chlorophyll absorption region [31,32]. It is, therefore, useful for plant species identification and mapping boundaries of soil types. The blue, green, and red bands sense within the visible spectrum where vegetation reflectance is based on chlorophyll absorption [31,33]. At the same time, soil reflectance at these wavebands tends to increase with wavelength based on texture, organic matter, and moisture content [31,32]. On the other hand, the NIR is responsive to the presence of vegetation biomass as chlorophyll is highly reflective in the NIR [32]. It can distinguish between dry and moist soils as water strongly absorbs the NIR [32]. Both the SWIR$_1$ and SWIR$_2$ are similarly sensitive to vegetation and soil moisture [33]. They are particularly useful for identifying disturbed soils and vegetation stress. As such, the configuration of

vegetation and soil spectral patterns along the visible and infrared wavelengths is a good indicator of the condition of the features on the ground [31].

The soil-adjusted vegetation index (SAVI) was also used to estimate and relate spectral behaviours with temporal biomass changes around the AWP. *SAVI* was calculated using Equation (1) [34]:

$$SAVI = \frac{NIR - RED}{NIR + RED} * (1 + L) \tag{1}$$

where

NIR = reflectance value of a pixel from the near-infrared band;

Red = reflectance value of a pixel from the red band; and

L = soil brightness correction factor. The *L* factor ranges between 0 for lowest-density vegetation and 1 for highest-density vegetation, and it is mostly defined as 0.5 to represent intermediate vegetation cover [34]. In this study, *L* is taken as 0.5 as it is recommended when studying soil-vegetation systems [35].

To account for drought events during the assessment period, an evapotranspiration dataset from the moderate resolution imaging spectroradiometer (MODIS) was obtained from the application for extracting and exploring analysis ready samples (AppEEARS) for the years 2002, 2012, 2018, 2020, and 2022. This was used to observe trends in evapotranspiration during the study dates.

2.6. Land Cover Classification around the AWP

We utilised a supervised learning approach to train the RF classifier in Google Earth Engine to map different land cover types on the reference image using field data collected at different sampling plots. As defined by Biau and Scornet [36], RF is a predictor consisting of a collection of randomised regression trees. The functionality of the RF classifier is based on an embedded feature assessment approach [37]. Its ability to perform better in terms of overall accuracy and kappa coefficient compared to other decision trees [38–40] has attracted wide-ranging utilisation in remote sensing applications [37]. Classification through this algorithm is achieved by combining several classification trees to perform ensemble learning [41]. The algorithm utilises the bootstrapping method to create sample datasets from training data on a random selection basis [37]. The sample datasets are then passed through each decision tree in a random forest to make predictions. The predictions from each decision tree in a forest are then aggregated on majority voting [37,42]. This process is called bagging, and the resultant classification follows Equation (2) [41]:

$$H(x) = argmaxy \sum_{i=1}^{K} I \tag{2}$$

where $H(x)$ is the final classification decision of the random forest; $hi(x)$ is the classification outcome in each decision tree *i*; *Y* is the output variable; and *I* is the indicative function [41].

Two parameters are needed for training the RF model for feature classification [41]. These are the number of trees (*ntree*) and the number of randomly selected features to be evaluated at each tree (*mtry*). These further determine the classification accuracy of the model [41,42]. In this study, 300 forest trees were used. Optimal accuracy is reported to be achieved from 200 trees onwards [39]. We also used the square root of the number of bands in each image to be classified as the number of randomly selected feature variables in this study. Land cover mapping using RF was performed at the vegetation species level based on the dominant species recorded at each sampling plot. A total of 261 training samples collected at the sampling plots were used to randomly train and validate the RF classifier in the Google Earth Engine. Some 80% of the training samples were used for training, while the remaining 20% were used for validation of the model on the 2022 Landsat image. The trained classifier was then applied to the 2020, 2018, 2012, and 2002 images to map land cover changes around the AWP before and after the installation of the water source.

Lastly, we used a *t*-test at a 95% confidence level to compare changes in different land covers at different distances before and after the introduction of the water point. The *t*-test is a statistical test that compares the means of two samples [43].

3. Results

3.1. Vegetation and Wildlife Diversity around the AWP

The vegetation species identified during the field survey are 38 woody trees and herbaceous plants. Key species included large-fruited jesse-bush combretum, camel thorn, mopane, sickle bush, false umbrella thorn, blackthorn, russet bushwillow and candle thorn. The Shannon–Wiener diversity index showed a low to moderate level of vegetation diversity (H) with a range of 1.52 to 2.43 in all directions. The species were distributed over a continuous surface of loose-grain thin Ferralic arenosols in all directions of the water point.

On the other hand, wildlife species identified in the study area totalled 17 species (Table 3). The species diversity ranged between 1.50 and 1.80. The highest species diversity of 1.80 was recorded within a 1 km radius of the AWP. However, the highest species abundance was observed within a 0.5 km radius of the AWP (Table 3). The most abundant species within this distance were zebra, impala, elephant, and buffalo at 58.1%, 7.0%, 6.2% and 5.4%, respectively. At a 1 km radius, the most abundant species were zebra at 29.5%, followed by impala at 26.1%, elephant at 17.0%, and roan at 12.5%. Elephant, zebra, roan, and impala maintained high species abundance at a 5 km radius of the AWP. Roan was the most abundant (37.5%) at 10 km radius of the AWP. This was followed by elephant (20.8%), dwarf mongoose (16.7%), and warthog (16.7%).

Table 3. Frequency and abundance of wildlife species encountered at various distances in the study area.

Wildlife Species	Frequency (0.5 km)	Abundance (%)	Frequency (1 km)	Abundance (%)	Frequency (5 km)	Abundance (%)	Frequency (10 km)	Abundance (%)
Zebra	75	58.1	26	29.5	6	22.2	0	0.0
Ostrich	2	1.6	0	0.0	0	0.0	0	0.0
Giraffe	2	1.6	0	0.0	0	0.0	0	0.0
Eland	4	3.1	2	2.3	0	0.0	0	0.0
Dwarf mongoose	3	2.3	2	2.3	3	11.1	4	16.7
Banded mongoose	1	0.8	0	0.0	0	0.0	0	0.0
Yellow mongoose	2	1.6	0	0.0	0	0.0	0	0.0
Impala	9	7.0	23	26.1	4	14.8	2	8.3
African buffalo	7	5.4	3	3.4	0	0.0	0	0.0
Wildebeest	5	3.9	1	1.1	0	0.0	0	0.0
Elephant	8	6.2	15	17.0	7	25.9	5	20.8
Warthog	1	0.8	5	5.7	0	0.0	4	16.7
Roan	6	4.7	11	12.5	6	22.2	9	37.5
Kudu	1	0.8	0	0.0	0	0.0	0	0.0
Jackal	1	0.8	0	0.0	0	0.0	0	0.0
Hyena	1	0.8	0	0.0	0	0.0	0	0.0
Lion	1	0.8	0	0.0	1	3.7	0	0.0

3.2. Vegetation and Soil Conditions

3.2.1. Spectral and Metabolic Changes at 0.5 km Distance from the Water Source

Spectral response patterns showed the reflectance of vegetation and soil features ranging between 27.8% and 67.6% across all wavelengths in 2002 (Figure 2a,b). In 2012, the reflectance decreased but at different rates ranging between 26.9% and 58.3% across

various bands of Landsat sensors (Figure 2a,b). Both features in both years displayed distinguishable spectral responses except in the near-infrared waveband. Notably, the spectral response of vegetation in both years deviated from the expected peak and valley behaviour for healthy green vegetation in the visible wavelengths. For example, a stronger reflection of red light by vegetation in 2002 and 2012 contradicted the expected strong absorption of radiation through chlorophyll for photosynthesis by healthy plants. This coincided with the lowest evapotranspiration rates of 126 mm and 313 mm in 2002 and 2012, respectively, compared to the years after the AWP.
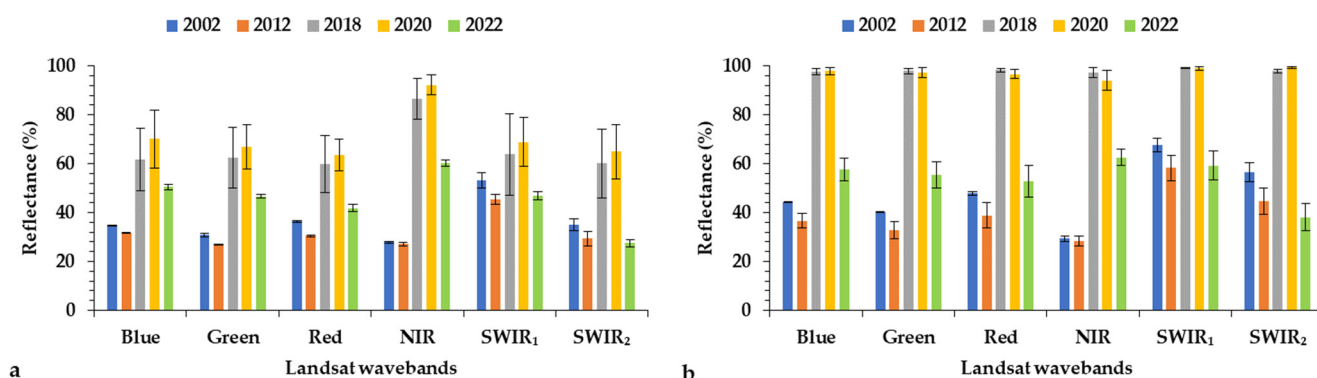
Figure 2. Spectral response patterns of (**a**) vegetation and (**b**) soil at 0.5 km distance from the AWP in 2002, 2012, 2018, 2020, and 2022.

In the years after the inception of the AWP (i.e., 2018 and 2020), the study area was characterised by extremely high reflectance across wavelengths by both vegetation and soil features (Figure 2a,b). The highest reflectance of nearly 100% was observed for soil features in all directions (Figure 2b, Table S2). However, photosynthetic activity was noticed in both years as characterised by the lowest reflection of red radiation within the visible spectrum and a peak reflection of NIR radiation. In contrast to 2018 and 2020, the reflection of radiation by vegetation and soil was suppressed across all wavebands in 2022 (Figure 2a,b). However, the reflection of energy across wavebands by both features remained higher than in the years before the AWP except in the SWIR ranges, matching the relatively high evapotranspiration rates in 2022 compared to 2002 and 2012. While vegetation was photosynthetically active in 2022, the spectral heterogeneity of both vegetation and soil was less distinctive across wavelengths compared to previous years (Figure 2a,b).

3.2.2. Spectral and Metabolic Changes at a 1 km Distance from the Water Source

The reflection range of vegetation and soil slightly declined by 7.6% in 2002 and 0.2% in 2012 while maintaining similar spectral patterns compared to a 0.5 km distance from the water source (Figure 3a,b). Both features also showed a slightly declined reflection of energy across wavelengths in 2018 and 2020 compared to shorter distances from the AWP. The decline was emphasised in 2018 in all directions (Figure 3b, Table S4). This was consistent with the highest evapotranspiration rate (429.7mm) observed in 2018. However, the SAVI index revealed that the relatively high moisture did not stimulate vegetation density, as the lowest indices (0.25 and 0.02) were recorded in the NE and N directions at this distance compared to the years before the AWP. On the other hand, vegetation and soil continued to show comparable spectral responses across wavelengths in 2022 (Figure 3a,b).
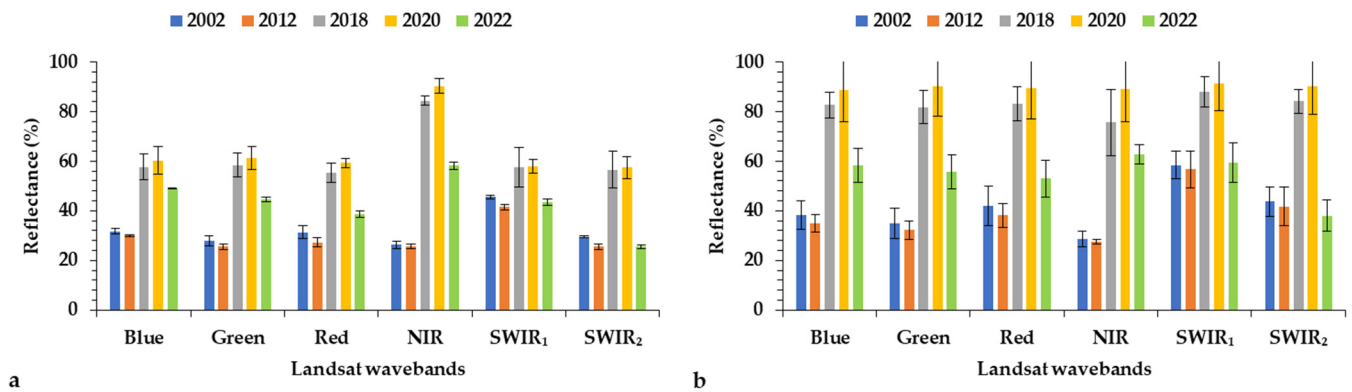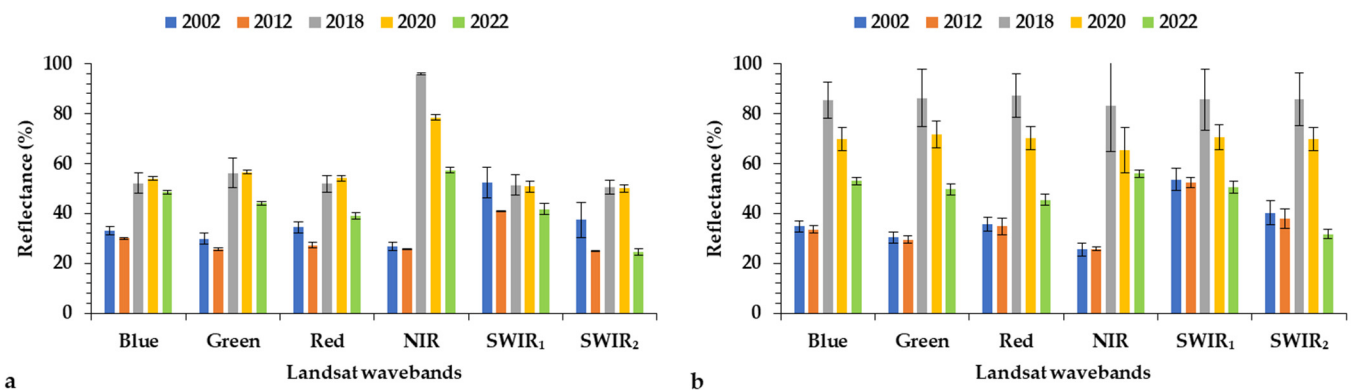
Figure 3. Spectral response patterns of (**a**) vegetation and (**b**) soil at a 1 km distance from the AWP in 2002, 2012, 2018, 2020, and 2022.

3.2.3. Spectral and Metabolic Changes at a 5 km Distance from the AWP

In 2002 and 2012, the reflection of energy by soil was mostly higher in the NE and NW directions than in the northern direction (Table S5). The state of aridity remained noticeable in different directions at this distance, chiefly characterised by a lack of photosynthetic behaviour in the visible wavelengths and some spectral overlaps of both vegetation and soil in some infrared wavelengths (Figure 4a,b, Table S5). The overlaps were mainly observed in the NE and NW directions.

Figure 4. Spectral response patterns of (**a**) vegetation and (**b**) soil at a 5 km distance from the AWP in 2002, 2012, 2018, 2020, and 2022.

The years 2018, 2020, and 2022 exhibited further improvement in the spectral response of features at a 5 km distance from the AWP compared to the same dates at shorter distances from the water source (Figure 4a,b). At this distance, the spectral improvements were much more noticeable on vegetation compared to soil (specifically soil in the NE and N directions, Figure 4b, Table S6). The most stable spectral behaviour was displayed by vegetation in the NW direction in 2018 and 2020 (Table S6). In contrast, the NE and N soils exhibited the highest reflection of visible light and SWIR radiations at this distance compared to the soils in NW (Table S6). In 2022, both features retained overly overlapping spectral responses across wavelengths in all directions, as observed at 0.5 km and 1 km away from the AWP (Figure 4a,b, Table S6).

3.2.4. Spectral and Metabolic Changes at a 10 km Distance from the Water Source

Despite the dry conditions and drought seasonality in 2002 and 2012, the reflection of energy at this distance by vegetation and soil remained lowest in both years compared to years after the AWP (Figure 5a,b). The reflection of energy by features ranged between 23.8% and 55.6% in 2002 and 23.9% and 48.8% in 2012.
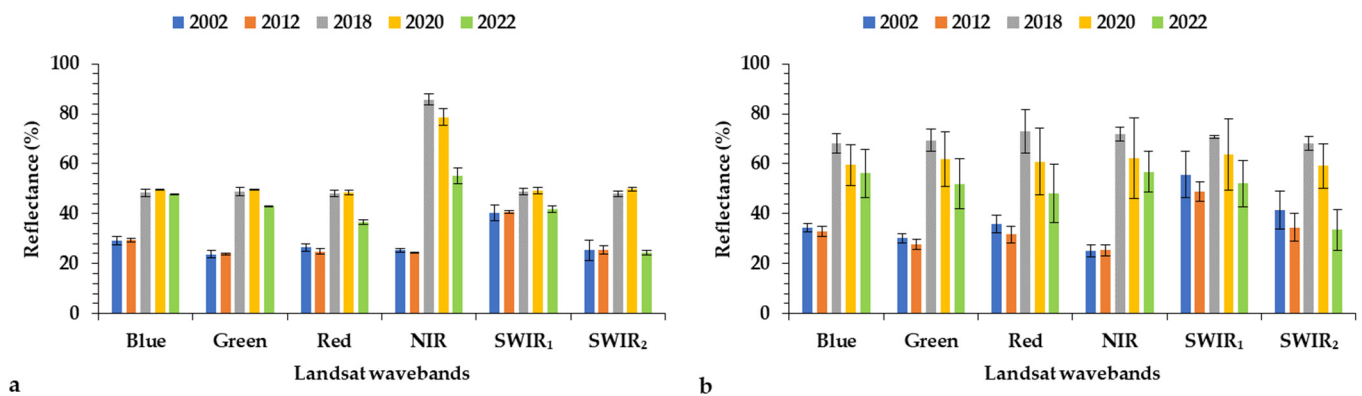
Figure 5. Spectral response patterns of (**a**) vegetation and (**b**) soil at a 10 km distance from the AWP in 2002, 2012, 2018, 2020, and 2022.

Reduced wildlife impacts on natural landscapes were noticeable by generally suppressed energy reflection by vegetation and soil in 2018, 2020, and 2022 (Figure 5a,b). However, environmental disturbances remained disproportionately intense over soil in the NE direction compared to soil in other directions in 2018 and 2020 (Table S8). In the same years, soil in the NE direction retained a high spectral response similar to the soil at a 5 km distance from the AWP while soil in the N direction exhibited a declining spectral response between 2018 and 2020 at this distance. On the other hand, the vegetation spectral response illustrated a photosynthesising vegetation cover in 2022. This is despite the maintained homogenisation of the landscape exhibited in 2022, as vegetation and soil spectral response patterns continued to strongly overlap across wavelengths (Figure 5a,b). Nonetheless, soil in the NW direction displayed a distinguishable spectral response compared to other features in other directions.

3.3. Land Cover Classification and Accuracies

The land cover types of the study area are shown in Figure 6, while Table 4 shows the error matrices, producer/user accuracies, kappa statistics, and overall accuracies of the trained RF classifier in 2022. The high number of correctly classified pixels in each land cover type as well as the high kappa statistic (0.75) and overall accuracy (80.6%) indicated that the RF model trained on Landsat imagery was effective in classifying land cover types in the study area (Table 4).

The trained RF model effectively classified land cover types in the study area into five major classes inclusive of woody and herbaceous species (Figure 6). These were (1) large-fruited jesse-bush combretum, camel thorn, black spear grass, wiregrass; (2) mopane, sickle bush, couch grass, common finger grass; (3) barren land; (4) false umbrella thorn, blackthorn, sickle bush, broad curly leaf; and (5) russet bushwillow, candle thorn, umbrella thorn, black spear grass.

Table 4. Random forest algorithm confusion matrix and accuracy assessment for the 2022 classified image.

Plant Communities	Large-Fruited Jesse-Bush Combretum Communities	Mopane Communities	Barren Land	False Umbrella Thorn Communities	Russet Bushwillow	Producer's Accuracy (%)	User's Accuracy (%)
Large-fruited jesse-bush combretum communities	**8**	2	0	0	0	80	53.3
Mopane communities	5	**13**	0	0	1	68.4	81.3
Barren land	0	0	**8**	0	0	100	100
False umbrella thorn communities	1	1	0	**14**	1	82.4	100
Russet bushwillow	1	0	0	0	**7**	87.5	77.8

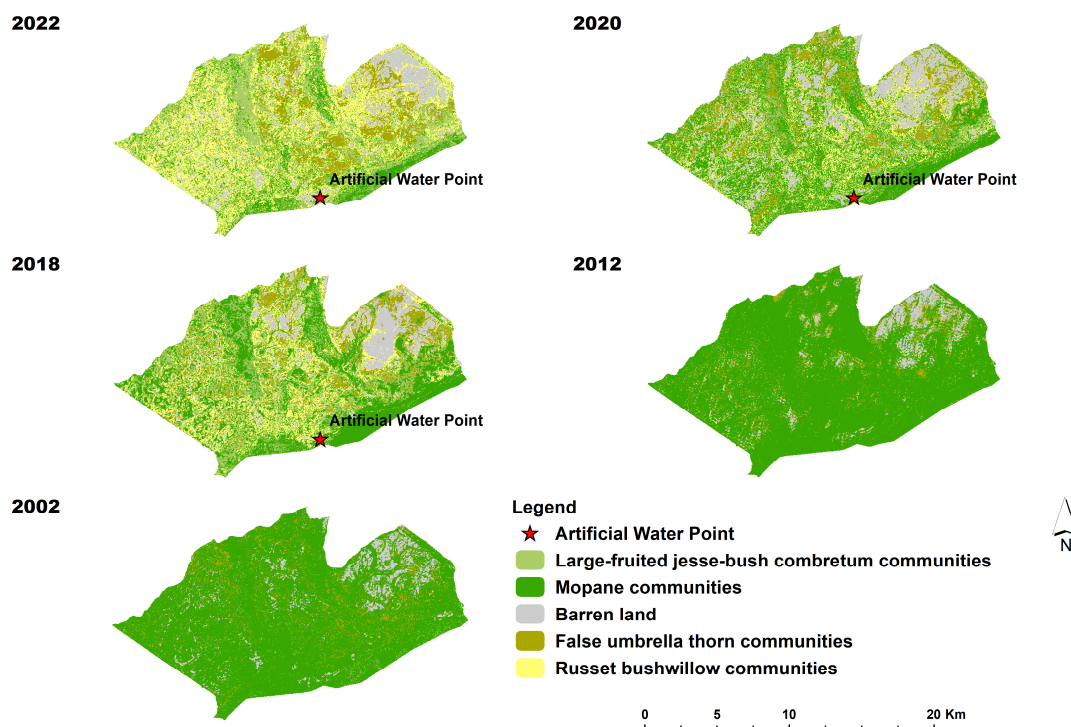Overall accuracy = 80.6%; kappa statistic = 75.3%.

Figure 6. Spatiotemporal landcover types in 2022, 2020, 2018, 2012, and 2002.

Diagonal elements (bolded) in Table 4 above show that the number of correctly classified pixels in each landcover class was higher than misclassified pixels. The RF model showed that most land cover classes were correctly classified at above 80% producer accuracies indicating high probabilities of correctly classified pixels for each land cover. At the same time, most of the landcover classifications were reliable and representative of the actual context at above 75% user accuracy.

Land cover maps revealed that the study area was historically dominated by mopane, sickle bush, couch grass, and common finger grass species in 2002 and 2012 (Figure 6, Table 5). The species showed the highest mean distribution at various distances compared to other land covers before the AWP (Table 5). However, the species declined significantly ($p = 0.075$) after the inception of the AWP within 0–0.5 km from the water point. A significant drop ($p = 0.048$), ($p = 0.019$), and ($p = 0.020$) was also seen at distances of 0.5–1 km, 1–5 km, and 5–10 km from the water source. Other plant communities demonstrated growing trajectories following the AWP. For example, russet bushwillow communities grew within 0–0.5 km of the water source (Table 5). The observed increase was statistically significant ($p = 0.023$) within this distance. A significant increase was also observed at 0.5–1 km ($p = 0.006$) and 1–5 km ($p = 0.022$) distances. At further distances (i.e., 5–10 km), the increase in russet bushwillow communities was not statistically significant with a *p*-value of 0.113. At the same time, the increase in large-fruited jesse-bush combretum communities after the introduction of the water point was not statistically significant, with $p = 0.255$ and $p = 0.105$ within 0–0.5 km and 0.5–1 km distances, respectively. Rather, the communities significantly increased with *p*-values of 0.002 and 0.011 within 1–5 km and 5–10 km, respectively. On the other hand, the increase in false umbrella thorn communities after the introduction of the water point was not statistically significant with *p*-values of 0.452, 0.594, and 0.216 within 0–0.5 km, 0.5–1 km and 1–5 km, respectively. Between 5 and 10 km distance from the water source, the species increased significantly ($p = 0.027$). Barren land also increased after AWP; however, the increase is not statistically significant with *p*-values of 0.483, 0.479, 0.119 and 0.069 at 0–0.5 km, 0.5–1 km, 1–5 km, and 5–10 km distances, respectively.

Table 5. Changes in the mean distribution (in km^2) of vegetation communities at various distances before and after the introduction of the AWP.

Land Cover	Area (in km^2)			
	0–0.5 km	0.5–1 km	1–5 km	5–10 km
Large-fruited jesse-bush combretum communities before AWP	0.01 ± 0.01	0.03 ± 0.03	0.64 ± 0.16	2.61 ± 0.95
Large-fruited jesse-bush combretum communities after AWP	0.08 ± 0.06	0.25 ± 0.10	9.03 ± 0.49	22.30 ± 2.85
Mopane communities before AWP	0.80 ± 0.08	1.55 ± 0.04	38.04 ± 0.74	86.74 ± 0.25
Mopane communities after AWP	0.25 ± 0.21	0.51 ± 0.33	14.82 ± 4.54	24.30 ± 12.55
Barren land before AWP	0.04 ± 0.02	0.10 ± 0.02	0.54 ± 0.10	7.58 ± 0.92
Barren land after AWP	0.15 ± 0.18	0.28 ± 0.30	1.66 ± 0.60	13.30 ± 2.05
False umbrella thorn communities before AWP	0.02 ± 0.001	0.03 ± 0.02	1.14 ± 0.49	6.26 ± 0.54
False umbrella thorn communities after AWP	0.04 ± 0.04	0.06 ± 0.07	3.87 ± 2.10	12.16 ± 1.28
Russet bushwillow communities before AWP	0	0	0.01 ± 0.02	0.19 ± 0.26
Russet bushwillow communities after AWP	0.19 ± 0.04	0.62 ± 0.07	10.97 ± 2.33	31.30 ± 16.16

4. Discussion

4.1. Vegetation and Wildlife Diversity around the AWP

The Shannon–Wiener diversity index showed that the study area hosts a diversity of vegetation and wildlife species. A total of 38 plant species were recorded with an overall low to moderate diversity index range of 1.52 to 2.43 in all directions from the water sources. The value of the Shannon–Wiener diversity index normally ranges between 1.5 and 3.5 [44]. This implies that the diversity of vegetation in our study area falls within the low to moderate values of species richness. This contrasts with the high vegetation diversity reported by Kashe et al. [45] and Mokatse et al. [20]. We partly attribute the low diversity established in this study to a smaller study extent utilised in our assessment compared to the previous studies. We also link the poor diversity to a reported continuous degradation of vegetation cover within the savanna landscape of Chobe by an increasing number of elephants and other herbivores [46].

A total of 23 animal species were also observed within the study area. Large and small herbivores and carnivore species were the main animal species identified within the peripheries of the AWP. The highest wildlife diversity was observed within a 1 km radius of the AWP. Herbivores such as zebra, impala, elephant, and buffalo were the most abundant within the study area mainly due to the established high and increasing population of herbivores in northern Botswana [14].

4.2. Vegetation and Soil Conditions

4.2.1. Spectral and Metabolic Changes at 0.5 km Distance from the Water Source

We observed a generally distinctive spectral heterogeneity between vegetation and soil in 2002 and 2012. This shows a maintained heterogeneous nature of the savanna landscape in both years [46]. However, vegetation spectra in both years in the visible wavelengths deviated from the expected reflectance patterns for living green vegetation as described by Lillesand et al. [31]. In this case, we noticed a peak reflection of red radiation in both years, which is contradictory to the expected strong absorption of the radiation by chlorophyll for photosynthesis. This implies that vegetation was photosynthetically inactive in both years. The lowest evapotranspiration rates of 126 mm and 313 mm recorded in 2002 and 2012, respectively, further imply that the study area experienced drought episodes that caused the prevalence of senescent foliage in the landscape. Vegetation conditions are enhanced by an increase in precipitation, as such moisture tends to be the most limiting factor for vegetation growth in arid and semi-arid landscapes [47].

Following the installation of the AWP, the highest reflection of energy by vegetation and soil was observed. A reflection of nearly 100% across wavelengths was noticed on soil features at this distance. The high reflection of energy by soils indicates their low moisture content. This is because the presence of moisture in the soil will decrease its reflectance due to the infrared absorption capabilities of water [31]. The introduction of AWPs causes the

gradual formation of piospheres as areas closer to the water points experience high grazing pressure and trampling as animals congregate at a reduced area [4]. The piospheres expose the ground surface to rapid moisture loss and further introduce changes in vegetation and soil conditions due to grazing gradients that form with continuous grazing pressure [4,5,46]. Our results also showed poor spectral heterogeneity between vegetation and soil following the installation of the AWP, consistent with the low to moderate vegetation diversity discussed. We attribute this to selective foraging of vegetation by some herbivores, e.g., elephants [12], and a gradual degradation of vegetation heterogeneity as wildlife numbers increase and grazing intensifies [8]. Our observations are consistent with Herrero et al. [46] who have shown that if savanna landscapes portray a nonequilibrium state, large ecological shifts may be induced by small- and large-scale shocks.

4.2.2. Spectral and Metabolic Changes at a 1 km Distance from the Water Source

Landscape conditions remained consistent in the study area in 2002 and 2012, as evidenced by consistent vegetation and soil spectral patterns at this distance from the water source. On the other hand, the low reflection of energy by vegetation and soil in the $SWIR_1$ and $SWIR_2$ wavelengths in 2018 compared to 2020 coincided with the highest evapotranspiration rate of 430 mm, indicating improved landscape moisture. We note that the improved moisture content could not restore landscape conditions at this distance, as shown by only a slight spectral change for both features compared to shorter distances and low SAVI indices. The findings indicate that wildlife disturbances associated with foraging and trampling persisted, reaching up to a 1 km distance from the water source, thereby corroborating the findings of Perkins [5] and Dzinotizei et al. [12] that the impact of piospheres may stretch beyond the immediate peripheries of AWPs, termed as the "sacrifice zone". The poor landscape condition restoration despite wetter conditions in 2018 confirms that the nonstrategic use of AWPs is detrimental to the resilience of semiarid landscapes, as their ecological functioning is disrupted by enhanced wildlife distribution through artificially altering water availability [1,9].

4.2.3. Spectral and Metabolic Changes at a 5 km Distance from the AWP

Noticeable spectral changes in vegetation and soil occurred in the NE and NW directions in 2002 and 2012. In this case, the reflection of energy by both features was mostly higher compared to the Northern direction, and spectral overlaps in some infrared wavelengths were noticed. The results implied that the features in the different directions were experiencing different landscape conditions at this distance. We attribute the portrayed spectral behaviour of features in the NE to the intensification of land use brought about by proximity to arable land and human settlements (i.e., Kachikau settlement). Intensification of land use causes a reduction of green cover, thereby accelerating drought severity through thermal and moisture stresses [47,48]. The higher spectral behaviour in the NW corresponds with a reduced moisture gradient in the NW direction. Reduced moisture influences strong reflectance, particularly within the infrared wavelengths, indicating that moisture content in vegetation leaves is also low [48].

In 2018 and 2020, the spectral behaviour of features improved for vegetation compared to soil at this distance. We noted a stable spectral behaviour by vegetation in the NW direction compared to other directions. We also noted that soil in NE and N exhibited the highest reflection of visible light and mid-infrared radiation compared to soil in NW. Both observations imply reduced landscape disturbances in the NW direction. The unique spectral response of vegetation and the implied less intense wildlife disturbance in the NW direction further suggest the onset of vegetation fragmentation in favour of the NW direction. This is because bushes in clusters surrounded by open areas tend to form in artificially altered landscapes due to intense browsing and the toppling of vegetation [49].

In 2022, the spectral behaviours of vegetation and soil retained overly overlapping trajectories across wavelengths in all directions, as initially observed at 0.5 km and 1 km away from the AWP. This signifies a homogenising landscape in 2022 attributed to an

increase in plants in dormant status as well as a change in the composition of the landscape. Vegetation stresses alter their spectral response patterns [31] while increasing density and foraging pressure by wildlife in areas with artificial water holes tend to cause long-term alterations in the configuration and composition of the landscapes through coppicing, thereby homogenising the landscapes [12].

4.2.4. Spectral and Metabolic Changes at a 10 km Distance from the Water Source

Consistency in spectral response patterns of vegetation and soil in 2002 and 2012 was maintained at this distance, further indicating minimal disturbances, and retained landscape heterogeneity before the installation of the AWP. Most importantly, the spectral consistency implies similar environmental conditions at varying sampling distances before the AWP. On the other hand, the spectral response patterns of features were generally suppressed in 2018, 2020, and 2022 across wavelengths at this distance compared to other distances except for soil in the NE direction. Landscape homogenisation also improved at this distance except in the NE direction. The reduction in the spectral response patterns at this distance shows reduced landscape disturbances, confirming that areas further away from AWPs experience less intense changes in landscape compositions, partly due to a decrease in animal density with distance from the AWP [50,51].

Lastly, our results reveal that the immediate years following the installation of an AWP are characterised by unstable spectral responses of features consistent with landscape disturbances that accompany the high-density aggregation of wildlife around the AWP. Later years, for example, 2022 in our study, show a stabilised spectral response by features, albeit strong homogenisation of the landscape attributable to a change in the composition of the landscape, increase in dead plant-based material and senescent foliage as more trees continue to be toppled and trampled in the area. The results also indicated an existing vulnerability of the study area to drought events with the potential of acting simultaneously with wildlife concentrations to aggravate AWP-induced disturbances on the landscape. Drought increases wildlife damage on woody vegetation, as such strategic water point closure is necessary to regulate grazing and reduce the wildlife pressure on the landscapes [52,53].

4.3. Land Cover Changes around the AWP

The overall accuracy and kappa statistic of our trained RF model for the classification of land cover in the study area were 80.6% and 0.75, respectively. This demonstrated the ability of supervised learning through the RF algorithm to accurately classify woody savanna landscapes in CE using Landsat imagery. Similarly, Kulkarni and Lowe [38] reported that RF showed better performance in terms of overall accuracy and kappa coefficient when compared with other classifiers. As such, the high accuracy of our model allows us to conclude that RF was effective in classifying land cover types in the study area into five major classes.

The results showed that the CE landscape consists of (1) large-fruited jesse-bush combretum, camel thorn, back spear grass, wiregrass; (2) mopane, sickle bush, couch grass, common finger grass; (3) barren land; (4) false umbrella thorn, blackthorn, sickle bush, broad curly leaf; and (5) russet bushwillow, candle thorn, umbrella thorn, black spear grass. The identification of woody and herbaceous species in this classification is in line with Sianga and Fynn [54] and Vittoz et al. [22] that vegetation communities in CE are characterised by different herbaceous and woody species with soil texture and fertility accounting for the species variations.

A comparison of land cover maps revealed that the inception of AWP initiated rapid land cover changes that disproportionately affected vegetation communities in the study area, particularly mopane woodlands. The woodlands exhibited significant ($p < 0.05$) declines within 0–10 km after the introduction of the water point. In this case, *Combretum*-dominated species, namely, large-fruited jesse-bush combretum communities, russet bushwillow communities, and barren land were shown to benefit from widespread decline

in mopane woodlands. The *Combretums* peaked significantly after the introduction of the water point at various distances from the water source. This is because the communities have a prolific resprouting attribute which is key to their resilience and productivity, particularly in disturbance-prone areas [55]. These are also most likely to persist under very high densities of herbivores due to their low palatability [56]. On the contrary, mopane woodlands have a low growth rate [57]. However, Vittoz et al. [22] indicated that the woodlands have a high nutritional value, with high protein and phosphorus contents, and as such, they attract intensive browsing by elephants. Mopane woodlands also provide suitable habitats for herbivorous species such as buffalo, roan, and sable antelope because of the abundance of digestible grasses that normally exist within the woodlands [22,54]. This causes the herbivore population to increase in these woodlands [54]. Therefore, the interplay of forage and habitat preference of the mopane woodlands by herbivore species and artificial alteration of surface water availability at these woodlands justifies their rapid reduction following the installation of the AWP in the study area.

5. Conclusions

Artificially manipulating surface water availability for wildlife in sub-tropical savannah ecosystems initiates wildlife-mediated effects on natural landscape configuration and composition through enhanced distribution patterns and high-density aggregations. Understanding how natural landscapes respond to alterations in surface water availability for wildlife can help inform the strategic use of artificial water resources and sustainably manage sub-tropical savannah ecosystems. The assessment of landscape variations following the installation of AWPs through multitemporal satellite imagery provides a unique opportunity to make direct landscape comparisons before and after the introduction of the resources. As a result, our study provides this opportunity in that spatiotemporal variation in landscape following the installation of an AWP in the CE was assessed using multitemporal Landsat images before and after the AWP. Our findings showed that the AWP in the CE instigated landscape disturbances on a drought-vulnerable landscape. The disturbances affected vegetation heterogeneity through the degradation of vegetation cover types. Immediate years following the AWP installation showed intense landscape disturbances consistent with sudden high-density aggregation of wildlife, whereas the landscapes strongly homogenised in later years due to the change in landscape composition, increase in dead plant-based material and senescent foliage as vegetation continued to be toppled and trampled. Our land cover classification model and *t*-test revealed that these disturbances disproportionately affected mopane woodlands compared to other land cover types. The study provides insights into how the continued nonstrategic use of AWPs and droughts in sub-tropical savannah ecosystems may induce large ecological shifts characterised by vegetation fragmentation and extinction of some species due to the detrimental effect on reproductive individuals and woody plant seedlings. However, there is a need for further studies looking at AWP impacts on natural landscapes using process-based climate models and hyperspectral satellite images to better detect non-photosynthetic plant material as a proxy for disturbances.

Supplementary Materials: The following supporting information can be downloaded at: https://www.mdpi.com/article/10.3390/land13050690/s1, Table S1: Percentage reflectance of vegetation and soil at a 0.5 km distance in different directions of AWP in 2002 and 2012; Table S2: Percentage reflectance of vegetation and soil at a 0.5 km distance in different directions of AWP in 2018, 2020, and 2022; Table S3: Percentage reflectance of vegetation and soil at a 1 km distance in different directions of AWP in 2002 and 2012; Table S4: Percentage reflectance of vegetation and soil at a 1 km distance in different directions of AWP in 2018, 2020, and 2022; Table S5: Percentage reflectance of vegetation and soil at a 5 km distance in different directions of AWP in 2002 and 2012; Table S6: Percentage reflectance of vegetation and soil at a 5 km distance in different directions of AWP in 2018, 2020, and 2022; Table S7: Percentage reflectance of vegetation and soil at a 10 km distance in different directions of AWP in 2002 and 2012; Table S8: Percentage reflectance of vegetation and soil at a 10 km distance in different directions of AWP in 2018, 2020, and 2022.

References

1. Bennitt, E.; Bradley, J.; Bartlam-Brooks, H.L.A.; Hubel, T.Y.; Wilson, A.M. Effects of artificial water provision on migratory blue wildebeest and zebra in the Makgadikgadi Pans ecosystem, Botswana. *Biol. Conserv.* **2022**, *268*, 109502. [CrossRef]
2. Rich, L.N.; Beissinger, S.R.; Brashares, J.S.; Furnas, B.J. Artificial water catchments influence wildlife distribution in the Mojave Desert. *J. Wildl. Manag.* **2019**, *83*, 855–865. [CrossRef]
3. Selebatso, M.; Maude, G.; Fynn, R.W.S. Assessment of quality of water provided for wildlife in the Central Kalahari Game Reserve, Botswana. *Phys. Chem. Earth. Parts A/B/C* **2018**, *105*, 191–195. [CrossRef]
4. Seletlo, Z. Vegetation and Soil Conditions around Water Points in Ranching and Communal Grazing Systems in the Hard Veld and Sandveld of Botswana. Master's Dissertation, Botswana University of Agriculture & Natural Resources, Gaborone, Botswana, 2017.
5. Perkins, J.S. Southern Kalahari piospheres: Looking beyond the sacrifice zone. *Land Degrad. Dev.* **2018**, *29*, 2778–2784. [CrossRef]
6. Makhabu, S.W.; Marotsi, B.; Perkins, J. Vegetation gradients around artificial water points in the Central Kalahari Game Reserve of Botswana. *Afr. J. Ecol.* **2002**, *40*, 103–109. [CrossRef]
7. Perkins, J.S. Changing the Scale and Nature of Artificial Water Points (AWP) Use and Adapting to Climate Change in the Kalahari of Southern Africa. In *Sustainability in Developing Countries: Case Studies from Botswana's Journey towards 2030 Agenda*; Keitumetse, S.O., Hens, L., Norris, D., Eds.; Springer: Cham, Switzerland, 2020; pp. 51–89. [CrossRef]
8. Croft, D.B. Walking in Each Other's Footsteps: Do Animal Trail Makers Confer Resilience against Trampling Tourists? *Environments* **2019**, *6*, 83. [CrossRef]
9. Mpolokang, M.O.; Perkins, J.S.; Saarinen, J.; Moswete, N.N. Environmental Change, Wildlife-Based Tourism and Sustainability in Chobe National Park, Botswana. In *Southern African Perspectives on Sustainable Tourism Management. Geographies of Tourism and Global Change*; Saarinen, J., Lubbe, B., Moswete, N.N., Eds.; Springer: Cham, Switzerland, 2022; pp. 169–185. [CrossRef]
10. Krag, C.; Havmøller, L.W.; Swanepoel, L.; Van Zyl, G.; Møller, P.R.; Havmøller, R.W. Impact of artificial waterholes on temporal partitioning in a carnivore guild: A comparison of activity patterns at artificial waterholes to roads and trails. *PeerJ* **2023**, *11*, e15253. [CrossRef] [PubMed]
11. Kasiringua, E.A. The Effects of Artificial Water Holes on the Distribution of Elephants and Other Mammalian Herbivores in Savuti, Northern Botswana. Master's Dissertation, Hedmark University College, Hedmark, Norway, 2010.
12. Dzinotizei, Z.; Murwira, A.; Masocha, M. Elephant-induced landscape heterogeneity change around artificial waterholes in a protected savanna woodland ecosystem. *Remote Sens. Appl. Soc. Environ.* **2019**, *13*, 97–105. [CrossRef]
13. Selebatso, M.; Bennitt, E.; Maude, G.; Fynn, R.W.S. Water provision alters wildebeest adaptive habitat selection and resilience in the Central Kalahari. *Afr. J. Ecol.* **2018**, *56*, 225–234. [CrossRef]
14. Chase, M.; Schlossberg, S.; Sutcliffe, R.; Seonyatseng, E. *Dry Season Aerial Survey of Elephants and Wildlife in Northern Botswana*; Elephants Without Borders: Kasane, Botswana, 2018.
15. Farrell, M.J.; Govender, D.; Hajibabaei, M.; van der Bank, M.; Davies, T.J. Environmental DNA as a management tool for tracking artificial waterhole use in savanna ecosystems. *Biol. Conserv.* **2022**, *274*, 109712. [CrossRef]
16. Wilson, L.J.; Hoffman, M.T.; Ferguson, A.J.; Cumming, D.H. Elephant browsing impacts in a Zambezian Baikiaea woodland with a high density of pumped waterholes. *Glob. Ecol. Conserv.* **2021**, *31*, e01854. [CrossRef]
17. Kolhoff, A.; Polet, G. *The Chobe Enclave: Non-Agricultural Activities, an Analysis*; University of Utrecht Geographical Institute: Utrecht, The Netherlands, 1990.

18. Stone, M.T. Community empowerment through community-based tourism: The case of Chobe Enclave Conservation Trust in Botswana. In *Institutional Arrangements for Conservation, Development and Tourism in Eastern and Southern Africa*; van der Duim, R., Lamers, M., van Wijk, J., Eds.; Springer: Dordrecht, The Netherlands, 2015; pp. 81–100. [CrossRef]

19. van der Sluis, T.; Cassidy, L.; Brooks, C.; Wolski, P.; VanderPost, C.; Wit, P.; Henkens, R.; van Eupen, M.; Mosepele, K.; Maruapula, O.; et al. *Chobe District Integrated Land Use plan*; Wageningen Environmental Research: Wageningen, The Netherlands, 2017. [CrossRef]

20. Mokatse, T.; Diaz, N.; Shemang, E.; Van Thuyne, J.; Vittoz, P.; Vennemann, T.; Verrecchia, E.P. Landscapes and Landforms of the Chobe Enclave, Northern Botswana. In *Landscapes and Landforms of Botswana. World Geomorphological Landscapes*; Eckardt, F.D., Ed.; Springer: Cham, Switzerland, 2022; pp. 91–116. [CrossRef]

21. Stone, M.T.; Nyaupane, G.P. Protected areas, wildlife-based community tourism and community livelihoods dynamics: Spiraling up and down of community capitals. *J. Sustain. Tour.* **2018**, *26*, 307–324. [CrossRef]

22. Vittoz, P.; Pellacani, F.; Romanens, R.; Mainga, A.; Verrecchia, E.P.; Fynn, R.W.S. Plant community diversity in the Chobe Enclave, Botswana: Insights for functional habitat heterogeneity for herbivores. *Koedoe Afr. Prot. Area Conserv. Sci.* **2020**, *62*, 1–17. [CrossRef]

23. Kaduyu, I.; Yuyi, G.; Kgosiesele, E. Identification of Areas for Sustainable Settlements in Highly Conflicted Protected Areas Using ArcGIS Spatial Analyst: A Case of Chobe District, Botswana. *J. Sustain. Dev.* **2021**, *14*, 84–98. [CrossRef]

24. Buckland, S.T.; Borchers, D.L.; Johnston, A.; Henrys, P.A.; Marques, T.A. Line Transect Methods for Plant Surveys. *Int. J. Biom.* **2007**, *63*, 989–998. [CrossRef]

25. Stephenson, P. Integrating Remote Sensing into Wildlife Monitoring for Conservation. *Environ. Conserv.* **2019**, *46*, 181–183. [CrossRef]

26. Barnett, D.T.; Stohlgren, T.J. A nested-intensity design for surveying plant diversity. *Biodivers. Conserv.* **2003**, *12*, 255–278. [CrossRef]

27. Jalonen, J.; Vanha-Majamaa, I.; Tonteri, T. Optimal sample and plot size for inventory of field and ground layer vegetation in a mature Myrtillustype boreal spruce forest. *Ann. Bot. Fenn.* **1998**, *35*, 191–196.

28. Ehlers, M. Spectral characteristics preserving image fusion based on Fourier domain filtering. In Proceedings of the Remote Sensing for Environmental Monitoring, GIS Applications, and Geology IV, Canary Islands, Spain, 22 October 2004. [CrossRef]

29. Ehlers, M.; Klonus, S.; Johan, A.; Rosso, P. Multi-sensor image fusion for pansharpening in remote sensing. *Int. J. Image Data Fusion* **2010**, *1*, 25–45. [CrossRef]

30. Al-Wassai, F.A.; Kalyankar, N.V.; Al-Zuky, A.A. The IHS Transformations Based Image Fusion. *arXiv* **2011**, arXiv:1107.4396. [CrossRef]

31. Lillesand, T.; Kiefer, R.W.; Chipman, J. *Remote Sensing and Image Interpretation*, 7th ed.; John Wiley & Sons: Hoboken, NJ, USA, 2015; pp. 12–17.

32. Tamouk, J.; Lotfi, N.; Farmanbar, M. Satellite image classification methods and Landsat 5TM Bands. *arXiv* **2013**, arXiv:1308.1801.

33. Mondejar, J.P.; Tongco, A.F. Near infrared band of Landsat 8 as water index: A case study around Cordova and Lapu-Lapu City, Cebu, Philippines. *Sustain. Environ. Res.* **2019**, *29*, 16. [CrossRef]

34. Hossain, M.S.; Khan, M.A.H.; Oluwajuwon, T.V.; Biswas, J.; Rubaiot, A.S.M.; Tanvir, M.S.S.I.; Munira, S.; Chowdhury, M.N.A. Spatiotemporal change detection of land use land cover (LULC) in Fashiakhali wildlife sanctuary (FKWS) impact area, Bangladesh, employing multispectral images and GIS. *Model. Earth Syst. Environ.* **2023**, *9*, 3151–3173. [CrossRef]

35. Zhen, Z.; Chen, S.; Yin, T.; Chavanon, E.; Lauret, N.; Guilleux, J.; Henke, M.; Qin, W.; Cao, L.; Li, J.; et al. Using the Negative Soil Adjustment Factor of Soil Adjusted Vegetation Index (SAVI) to Resist Saturation Effects and Estimate Leaf Area Index (LAI) in Dense Vegetation Areas. *Sensors* **2021**, *21*, 2115. [CrossRef] [PubMed]

36. Biau, G.; Scornet, E. A random forest guided tour. *TEST* **2016**, *25*, 197–227. [CrossRef]

37. Ma, L.; Fu, T.; Blaschke, T.; Li, M.; Tiede, D.; Zhou, Z.; Ma, X.; Chen, D. Evaluation of Feature Selection Methods for Object-Based Land Cover Mapping of Unmanned Aerial Vehicle Imagery Using Random Forest and Support Vector Machine Classifiers. *ISPRS Int. J. Geo-Inf.* **2017**, *6*, 51. [CrossRef]

38. Kulkarni, A.D.; Lowe, B. Random forest algorithm for land cover classification. *Int. J. Recent Innov. Trends Comput. Commun.* **2016**, *4*, 58–63.

39. Gunčar, G.; Kukar, M.; Notar, M.; Brvar, M.; Černelč, P.; Notar, M.; Notar, M. An application of machine learning to haematological diagnosis. *Sci. Rep.* **2018**, *8*, 411. [CrossRef] [PubMed]

40. Parmar, A.; Katariya, R.; Patel, V. A review on random forest: An ensemble classifier. In Proceedings of the International Conference on Intelligent Data Communication Technologies and Internet of Things (ICICI), Coimbatore, India, 7 August 2018. [CrossRef]

41. Wang, Z.; Zhao, Z.; Yin, C. Fine crop classification based on UAV hyperspectral images and random forest. *ISPRS Int. J. Geo-Inf.* **2022**, *11*, 252. [CrossRef]

42. Ming, D.; Zhou, T.; Wang, M.; Tan, T. Land cover classification using random forest with genetic algorithm-based parameter optimization. *J. Appl. Remote Sens.* **2016**, *10*, 035021. [CrossRef]

43. Kang, H. Sample size determination and power analysis using the G*Power software. *J. Educ. Eval. Health Prof.* **2021**, *18*, 17. [CrossRef]

44. Ortiz-Burgos, S. Shannon-Weaver Diversity Index. In *Encyclopedia of Estuaries, Encyclopedia of Earth Science Series*; Kennish, M.J., Ed.; Springer: Dordrecht, The Netherlands, 2016; pp. 572–573. [CrossRef]
45. Kashe, K.; Teketay, D.; Mmusi, M.; Kemosedile, T.; Galelebalwe, M.K. Assessment of diversity and composition of tree species in residential areas of Chobe district, northern Botswana. *Agric. For.* **2022**, *68*, 233–245. [CrossRef]
46. Herrero, H.V.; Southworth, J.; Bunting, E. Utilizing Multiple Lines of Evidence to Determine Landscape Degradation within Protected Area Landscapes: A Case Study of Chobe National Park, Botswana from 1982 to 2011. *Remote Sens.* **2016**, *8*, 623. [CrossRef]
47. Jiang, T.; Su, X.; Singh, V.P.; Zhang, G. Spatio-temporal pattern of ecological droughts and their impacts on health of vegetation in Northwestern China. *J. Environ. Manag.* **2022**, *305*, 114356. [CrossRef]
48. Taiwo, B.E.; Kafy, A.A.; Samuel, A.A.; Rahaman, Z.A.; Ayowole, O.E.; Shahrier, M.; Duti, B.M.; Rahman, M.T.; Peter, O.T.; Abosede, O.O. Monitoring and predicting the influences of land use/land cover change on cropland characteristics and drought severity using remote sensing techniques. *Environ. Sustain. Indic.* **2023**, *18*, 100248. [CrossRef]
49. Sterk, M.; Cubas, F.S.; Reinhard, B.; Reinhard, F.; Kleopas, K.; Jewell, Z. The importance of large pans and surrounding bushveld for black rhino (*Diceros bicornis* ssp. *bicornis*) habitat use in the Kalahari: Implications for reintroduction and range expansion. *Namib. J. Environ.* **2023**, *7*, 1–13.
50. Åldemo, C. Effects of Elephants and Other Browsers on Woody Vegetation around Artificial Waterholes in Savuti, Northern Botswana. Master's Dissertation, Uppsala University, Uppsala, Sweden, 2011.
51. Mukwashi, K.; Gandiwa, E.; Kativu, S. Impact of African elephants on Baikiaea plurijuga woodland around natural and artificial watering points in northern Hwange National Park, Zimbabwe. *Int. J. Environ. Sci.* **2012**, *2*, 1355. [CrossRef]
52. Thornley, R.; Spencer, M.; Zitzer, H.R.; Parr, C.L. Woody vegetation damage by the African elephant during severe drought at Pongola Game Reserve, South Africa. *Afr. J. Ecol.* **2020**, *58*, 658–673. [CrossRef]
53. Graz, F.P.; Westbrooke, M.E.; Florentine, S.K. Modelling the effects of water-point closure and fencing removal: A GIS approach. *J. Environ. Manag.* **2012**, *104*, 186–194. [CrossRef]
54. Sianga, K.; Fynn, R. The vegetation and wildlife habitats of the Savuti-Mababe-Linyanti ecosystem, northern Botswana. *Koedoe Afr. Prot. Area Conserv. Sci.* **2017**, *59*, 1–16. [CrossRef]
55. Kalema, V.N. Diversity, use and resilience of woody species in a multiple land use Equatorial African Savanna, Central Uganda. Ph.D. Thesis, University of the Witwatersrand, Johannesburg, South Africa, 2010.
56. Archibald, S.; Twine, W.; Mthabini, C.; Stevens, N. Browsing is a strong filter for savanna tree seedlings in their first growing season. *J. Ecol.* **2021**, *109*, 3685–3698. [CrossRef]
57. Tabares, X.; Zimmermann, H.; Dietze, E.; Ratzmann, G.; Belz, L.; Vieth-Hillebrand, A.; Dupont, L.; Wilkes, H.; Mapani, B.; Herzschuh, U. Vegetation state changes in the course of shrub encroachment in an African savanna since about 1850 CE and their potential drivers. *Ecol. Evol.* **2020**, *10*, 962–979. [CrossRef] [PubMed]